Oxidation Resistance and Emissivity of Diboride-Based Composites Containing Tantalum Disilicide in Air Plasma up to 2600 K for Space Applications

C. Pellegrini, M. Balat-Pichelin, O. Rapaud, E. Bêche

Ceramics International 48 (2022) 27878–27890

Contents lists available at ScienceDirect

Ceramics International

journal homepage: www.elsevier.com/locate/ceramint

Oxidation resistance and emissivity of diboride-based composites containing tantalum disilicide in air plasma up to 2600 K for space applications

C. Pellegrini [a,b], M. Balat-Pichelin [a,*], O. Rapaud [b], E. Bêche [a]

[a] PROMES-CNRS, UPR8521, 7 rue du four solaire, 66120 Font-Romeu Odeillo, France
[b] IRCER-CNRS, UMR 7315, Centre Européen de la Céramique, 12 Rue Atlantis, 87068, Limoges, France

ARTICLE INFO

Keywords:
UHTC
Oxidation
Air plasma
High temperature
Space applications

ABSTRACT

Fully-dense ZrB_2 and HfB_2 composites were elaborated by Spark Plasma Sintering with 20 vol% $TaSi_2$ to replace SiC in the aim of improving their oxidation resistance. This study follows the one carried out on (Zr/Hf)B_2–SiC systems in the same oxidation conditions. The oxidation behavior of ZrB_2–20%$TaSi_2$ and HfB_2-20%$TaSi_2$ in air plasma conditions, at 1000 Pa total pressure and from 1950 K up to 2600 K, was studied using the MESOX facility implemented at the focus of the 6 kW Odeillo solar furnace. The mass variation of the samples during an oxidation duration of 300 s on a temperature plateau was followed. A four step oxidation mechanism is proposed. A good oxidation behavior, with a slight mass gain, has been identified up to 2170 K due to the formation of a refractory mixed oxide $(Hf/Zr)_6Ta_2O_{17}$ at the surface of the samples. An improvement of the oxidation resistance by 200 K is obtained compared to the composites with SiC as additional compound. Moreover, as emissivity is an important parameter for space applications and that oxidation plays a huge role on the evolution of the emissivity, the normal spectral emissivity was measured on several pre-oxidized samples using atomic oxygen (representative surfaces) and the normal total emissivity was calculated. Finally, for both the compositions, the emissivity is comprised between 0.80 and 0.90 in the temperature range 1300–2200 K.

1. Introduction

Ultra-high temperature ceramics (UHTCs), among them the borides ZrB_2 and HfB_2, are promising for extreme environments due to their good oxidation behavior at high temperatures (more than 2000 K) under oxidizing atmosphere. Additional compounds have been considered to improve their oxidation resistance. The most common in the literature is silicon carbide as developed in our previous paper [1].

The oxidation behavior of diboride-based composites with $TaSi_2$ as additional compound has been studied with samples prepared using different sintering methods (mostly Hot Pressing and also Spark Plasma Sintering, simplified by HP or SPS respectively) and in different conditions, sometimes away from the application ones. Hypersonic atmospheric re-entry conditions on Earth include low oxygen partial pressure, atomic oxygen, and temperatures higher than 2000 K. In the following sections, the literature relative to the oxidation of these composites has been summarized according to the composition, $TaSi_2$ with or without SiC - a large part of the studies being made on (Zr/Hf)B_2–SiC systems with $TaSi_2$ as additional compound.

1.1. Oxidation of (Zr/Hf)B_2–SiC composites with $TaSi_2$ as additional compound

Justin and Jankoviak have oxidized (Hf/Zr)B_2-20 vol% SiC-20 vol% $TaSi_2$ composites at 1773 K by arc-jet during 600 s for the ATLLAS project, which consisted to design a civil aircraft for hypersonic flights [2]. The materials have shown a good oxidation behavior up to 1773 K due to the formation of a glassy protective layer on the surface that could slow down the diffusion of oxygen. Opila et al. have oxidized ZrB_2-20 vol % SiC-20 vol% $TaSi_2$ composites – sintered by HP – in an arc-jet facility at 2163 K for 10 min [3]. It appears that the $TaSi_2$ addition seems not beneficial for the oxidation resistance of the composite at this temperature due to the formation of a liquid phase on the surface, composed of 6 $ZrO_2.Ta_2O_5$ (mixed oxide $Zr_6Ta_2O_{17}$) based on EDS analysis. According to these authors, this mixed oxide would have a melting temperature around 2000 K that is much lower than the melting temperature of the

* Corresponding author.
E-mail address: Marianne.balat@promes.cnrs.fr (M. Balat-Pichelin).

https://doi.org/10.1016/j.ceramint.2022.06.090
Received 8 March 2022; Received in revised form 31 May 2022; Accepted 8 June 2022
Available online 11 June 2022

Table 1
Compositions and imposed temperatures during the SPS cycle.

Sample name	H80T20	Z80T20
Diboride (ZrB_2 or HfB_2) content (vol%)	80	80
$TaSi_2$ content (vol%)	20	20
Imposed temperature (K)	1873	1823

mixed oxide $Hf_6Ta_2O_{17}$ established at 2523 K by Mc Cormack et al. [4]. Gasch and Johnson studied the oxidation of HfB_2-10 vol% SiC-5 vol% $TaSi_2$, sintered by two methods, HP or SPS, in an arc-jet facility under a heat flux of 250 W/cm^2 for 5 min [5]. They concluded that the samples sintered by SPS shown a better oxidation behavior with a smaller oxide layer than those sintered by HP. It also appears that $TaSi_2$ improved the oxidation resistance under dissociated atmosphere because the thickness of the oxide layer was divided by 3, certainly due to the small grain size after sintering allowed by the $TaSi_2$ addition. Opila et al. have also oxidized (Hf/Zr)B_2-based samples with SiC and tantalum compounds ($TaSi_2$ and TaC) in a furnace under stagnant air at 1900 K for several 10 min cycles: 1, 5 and 10 cycles [3]. The tantalum-based compositions were compared to those containing only SiC under the same oxidation conditions. They concluded that the addition of 20 vol% $TaSi_2$ to ZrB_2/SiC significantly improved the oxidation resistance at 1900 K. This improvement was attributed to the presence of Ta, although the mechanism was not yet understood at that time. In addition, TaC would not have the same beneficial effects as $TaSi_2$ and $TaSi_2$ has no effect on the HfB_2/SiC composites. Among the studies of borides associated with tantalum compounds, the study of Simonenko et al. differed because the HfB_2-SiC-Ta_4HfC_5 composites produced by reactive HP (relative density of 81.5%) were oxidized under atomic oxygen at 2123 K for 2000 s [6]. After oxidation, a significant mass gain of 5.9% was observed. For comparison with previous studies, Simonenko et al. recalled that the mass loss was 1.7% for HfB_2-30 vol% SiC-5 vol% $Y_3Al_5O_{12}$ samples and 8.6% for porous HfB_2-65 vol% SiC samples. The addition of a tantalum compound seems to have a beneficial effect on the oxidation resistance under dissociated atmosphere due to the formation of a stable $Hf_6Ta_2O_{17}$

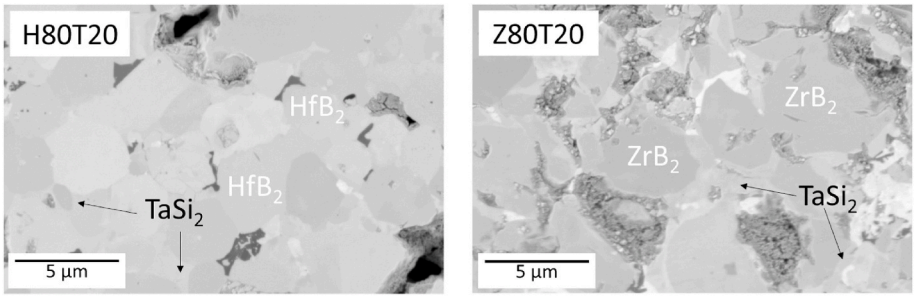

Fig. 1. SEM images of the H80T20 and Z80T20 surfaces after SPS.

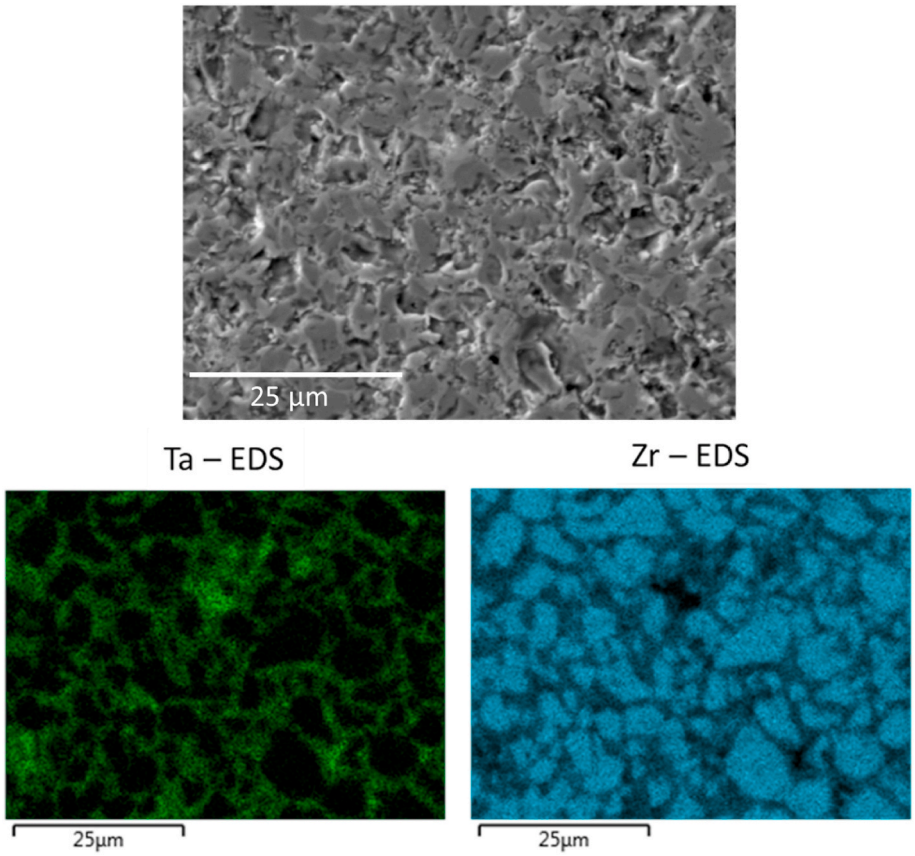

Fig. 2. SEM image and EDS mapping of a sintered Z80T20 sample before oxidation.

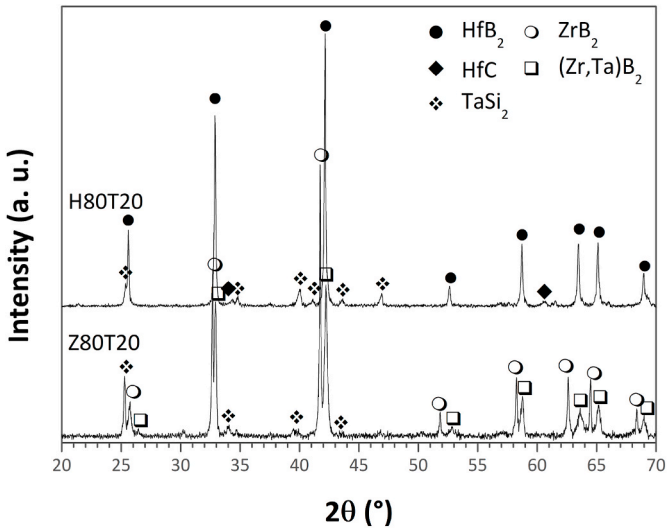

Fig. 3. XRD patterns of the H80T20 and Z80T20 samples after sintering.

mixed oxide.

1.2. Oxidation of $(Zr/Hf)B_2$–$TaSi_2$ composites without SiC

Silvestroni et al. conducted a comparative study on the oxidation resistance of ZrB_2 with 15 vol% of several disilicides as additional compounds: $MoSi_2$, $TaSi_2$, WSi_2 and $ZrSi_2$ from 1473 to 1923 K during 15 min in a furnace in air [7]. Up to 1773 K, the composition with $TaSi_2$ has one of the thinnest oxide layers compared to the others. It seems that $TaSi_2$ provided a good protection against oxidation. Talmy et al. have highlighted, after oxidation, the presence of a glassy phase on the surface composed of a mixed oxide Zr–Ta–O on similar compounds [8,9]. According to Silvestroni et al., the presence of Ta would even be harmful because of a volume expansion due to the formation of a mixed oxide of zirconium and tantalum. However, Talmy et al. arrived to an opposite conclusion for tantalum as additional compound. Indeed, the presence of Ta would have a beneficial effect because the mixed oxide that formed on the surface was viscous and covered the entire surface of the material, which greatly limited the diffusion of oxygen within the material. Silvestroni and Kleebe have oxidized ZrB_2-15 vol% $TaSi_2$ composite at 1773 K and 1923 K in a furnace previously heated to the targeted temperature under stagnant air during 15 min [10]. Upon oxidation, this composite formed a multilayer architecture in the oxide layer. At 1773 K, the extreme surface was composed of $TaZr_{2.75}O_8$ platelets immersed in a thin film of silica glass, and the bottom layer was composed of ZrO_2 partially filled with glass and enveloping TaB_2 grains. The authors have observed that the Ta compounds were transformed into solid Ta_2O_5 and this transformation was accompanied by a volume expansion that caused a breach at the interface between the oxide layer and the un-oxidized material with the increase of the temperature up to 1923 K. Hu et al. have studied the impact of several additional compounds: TiB_2, HfB_2, CrB_2, TaB, $TaSi_2$, LaB_6, La_2O_3, and AlN on the oxidation resistance of ZrB_2-based composites [11]. They have oxidized a ZrB_2-20 vol% $TaSi_2$ sample in a furnace under stagnant air for 1 h at 2023 K. The sample was totally consumed during this time, only a pink oxide shell remained after oxidation. After comparison with the monolithic ZrB_2 sample oxidized under the same conditions, it seems that the addition of $TaSi_2$ is deleterious for the oxidation resistance as its behavior was much worse but no explanation was given by the authors at that time. Sciti et al. have oxidized HfB_2-15 vol% $TaSi_2$ by arc-jet between 2273 K and 2773 K [12]. At temperatures above 2273 K, it seems that $TaSi_2$ is not the expected candidate. Ta was foreseen as an ideal candidate to modify the nature of the hafnia layer at the surface by introducing oxygen into the lattice to stabilize the oxide in its quadratic/cubic form. This stabilization would have prevented the volume expansion upon cooling and thus cracking leading to the detachment of the protective oxide layer on the surface. However, the study of Sciti et al. has shown that for a composite containing 15 vol% $TaSi_2$, the most obvious evolution of the oxide layer on the surface is the formation of the $Hf_6Ta_2O_{17}$ phase which tends to detach when the temperature exceeds 2273 K. In addition, $TaSi_2$ appears to promote the formation of a porous layer below the surface, making

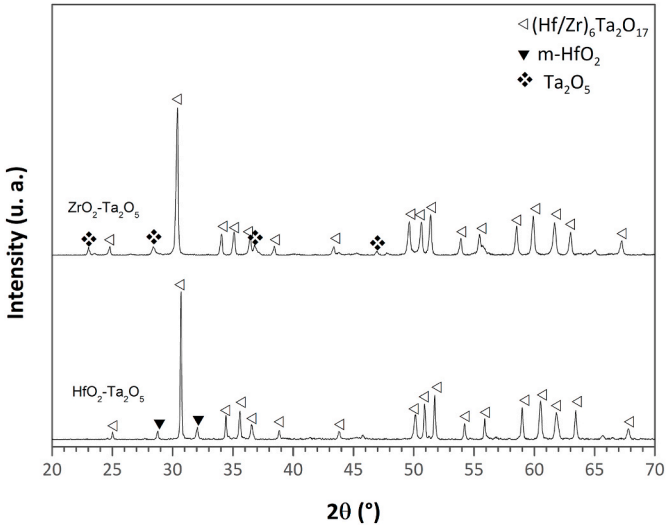

Fig. 5. XRD patterns of the $(Hf/Zr)O_2$–Ta_2O_5 samples after sintering in the MESOX set-up.

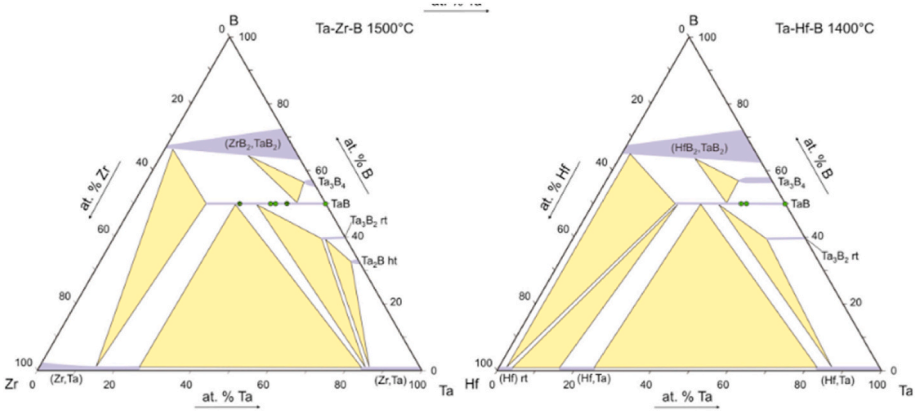

Fig. 4. Ternary phases diagrams (Zr,Hf)-Ta-B (from Ref. [18]).

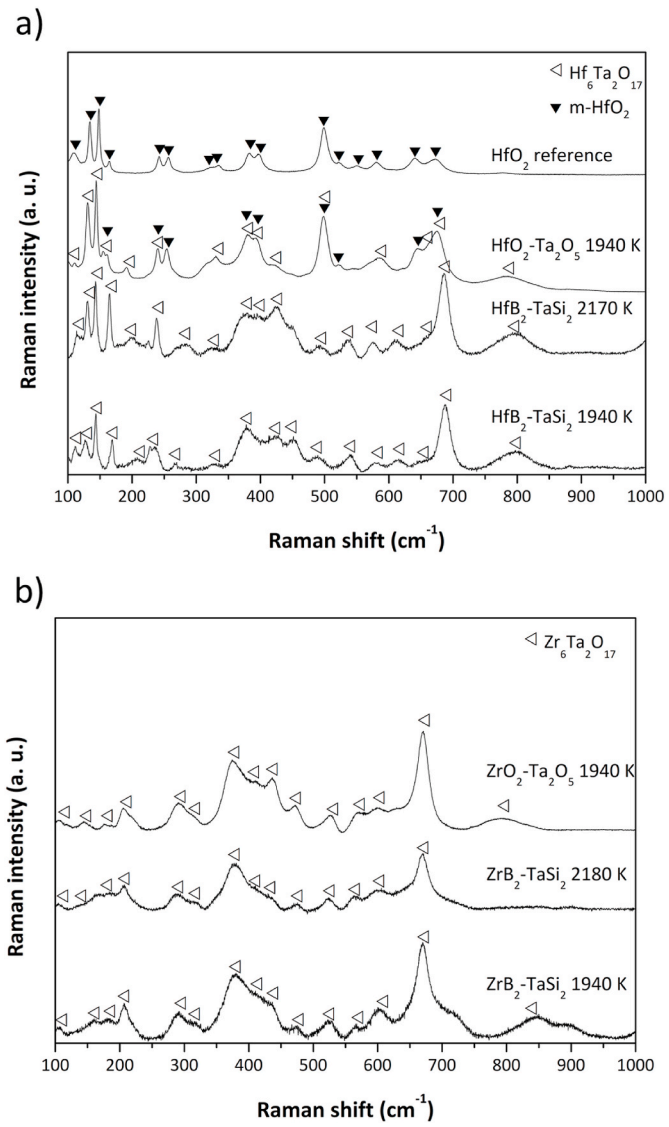

Fig. 6. Raman spectra of the mixed oxides: a) $Hf_6Ta_2O_{17}$ and b) $Zr_6Ta_2O_{17}$ obtained on the oxidized samples at the temperatures mentioned and of the sintered oxides at 1940 K in the MESOX set-up.

the material permeable to oxidation.

1.3. Aim of our study

Our study brings a new light on the oxidation behavior of (Hf/Zr)B_2–$TaSi_2$ composites by combining fully-dense materials sintered by SPS – with optimized parameters to avoid the detrimental effect of porosity

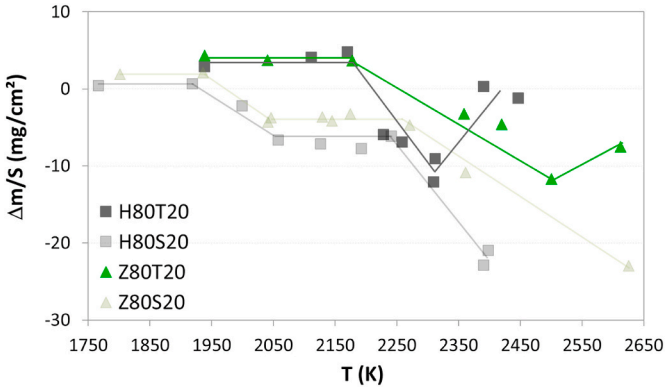

Fig. 8. Mass variation per unit area versus temperature for the two studied compositions containing $TaSi_2$ and results for (Hf/Zr)B_2–SiC composites obtained in a previous study in gray levels [1].

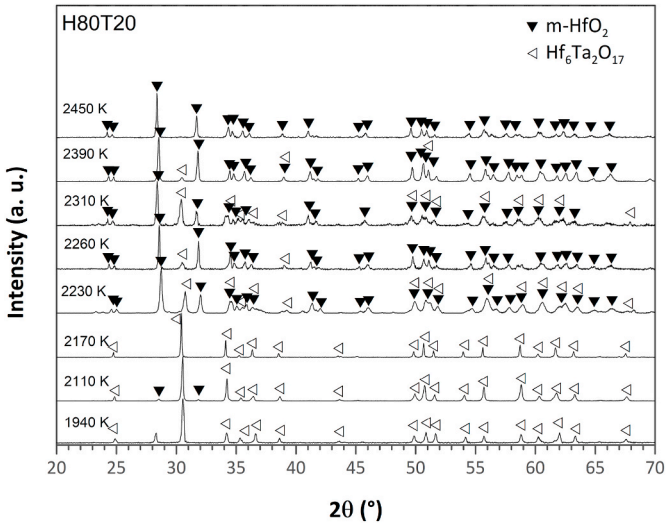

Fig. 9. XRD patterns for the H80T20 samples after oxidation.

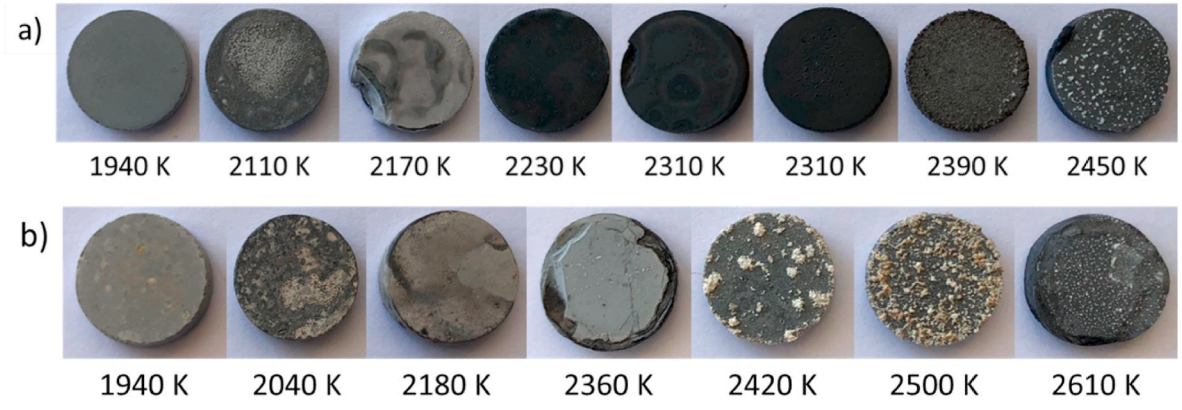

Fig. 7. Photos of the samples after oxidation in air plasma during 300 s in the 1940–2610 K temperature range for a) H80T20 and b) Z80T20 composites.

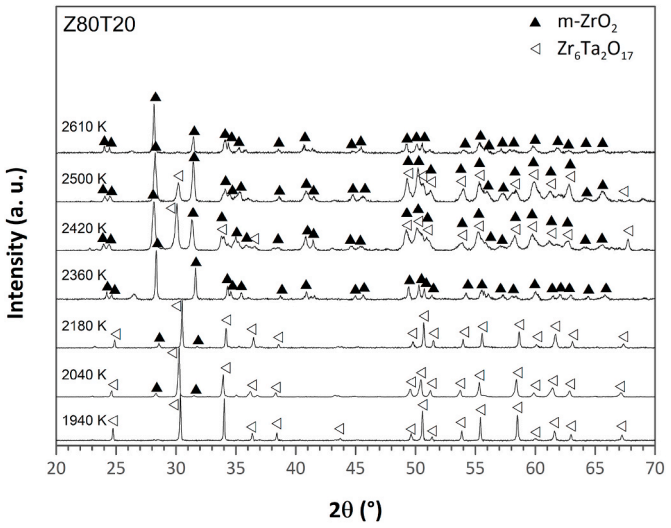

Fig. 10. XRD patterns for the Z80T20 samples after oxidation.

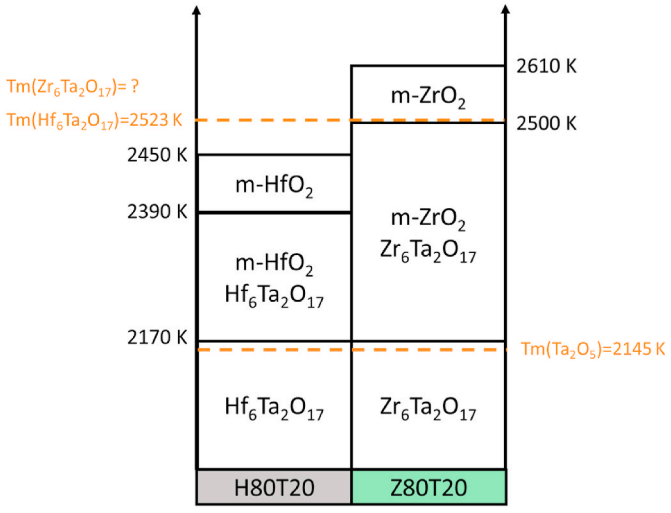

Fig. 11. Summary of the identified phases by XRD for the H80T20 and Z80T20 composites according to the temperature level.

on their oxidation resistance –, low total pressure, atomic oxygen, temperature greater than 2000 K which is different from the existing literature. The aim of this work is to study the oxidation mechanisms occurring in a large domain of temperature, from 1950 K up to 2600 K, in air plasma conditions for diboride-based composites containing 20 vol % $TaSi_2$ with fully-dense microstructure obtained by SPS. Using different characterization techniques after oxidation such as SEM, XRD and Raman spectroscopy, we have proposed a four-step oxidation mechanism in the whole temperature range that has never been proposed in the literature. This study follows the one on the oxidation of (Zr/Hf)B_2 with SiC as additional compound, carried out in the same conditions [1]. Moreover, the measurement of the total emissivity was performed as it is an important parameter for aerospace applications, because the hot parts of the vehicle can be submitted to extreme temperatures during a hypersonic reentry and the materials must have a high emissivity to reject the heat absorbed. It is well-known that oxidation plays a huge role on the evolution of the emissivity, this is why we have measured the normal spectral emissivity and calculated by integration the values of the normal total emissivity obtained on pre-oxidized samples in air plasma conditions that are more representative of the surface state of the heat shield materials of a space vehicle.

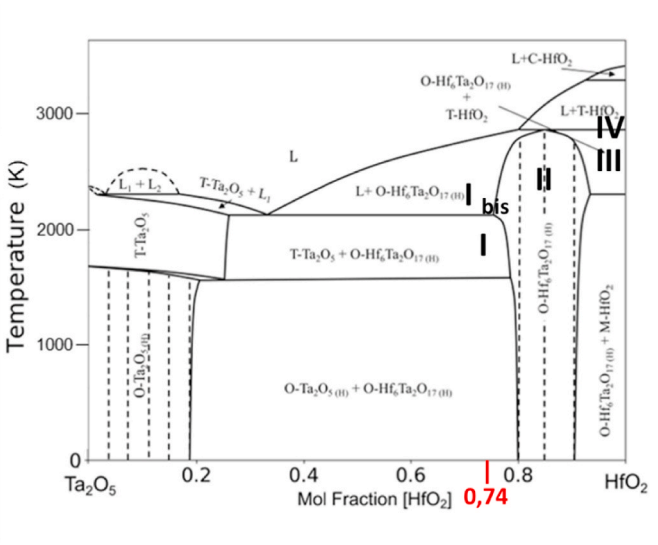

Fig. 12. HfO_2-Ta_2O_5 phase diagram (from Ref. [4]) with the four concerned domains (I to IV).

2. Materials and methods

In this section, the sample elaboration, the oxidation method, the emissivity measurement and the material characterization are presented.

2.1. Sample elaboration

Commercial powders, HfB_2 powder (99.5% purity, $d_{50} = 22$ µm, $\rho = 11$ g cm^{-3}, from abcr, Germany), ZrB_2 powder (97% purity, $d_{50} = 5.7$ µm, $\rho = 6$ g cm^{-3}, from H.C. Starck, Germany) and $TaSi_2$ powder (99.0 % purity, −325 mesh, $\rho = 9.14$ g cm^{-3}, abcr, Germany) were chosen as raw materials. The grain size of the HfB_2 powder has been refined by planetary milling. The HfB_2 powder was grinded up to a d_{50} value of 5.4 µm before sintering to control the microstructure and to obtain an equivalent grain size on each composite. The $TaSi_2$ powder was also refined to reach a d_{50} value of 6.5 µm. The ZrB_2 powder already has the required size. WC balls were used in a WC media for planetary milling.

The powder mixtures were introduced in a graphite die (inner diameter of 13 mm for oxidation study and of 25 mm for emissivity measurement) lined with a graphitized paper (Papyex, Mersen, France), then pre-compacted at 75 MPa, and sintered using Spark Plasma Sintering (Dr Sinter 825, Fuji Electronics Industrial Co. Ltd., Japan). The temperature was monitored by an optical pyrometer at the external surface of the die. Sintering parameters were optimized depending on the type of diboride (Table 1). Fully dense samples were obtained with optimized conditions (holding time, temperature, applied load). Every sintering cycle was carried out in vacuum, using a heating rate of 100 K min^{-1} with an applied load of 100 MPa and 10 min of holding time. To simplify the names of the composites, H or Z and T letters, attributed to the HfB_2 or ZrB_2 and $TaSi_2$ phases respectively, were followed by the volume percent of HfB_2 or ZrB_2 and $TaSi_2$ constituting the composite. The bulk density was measured using the method based on Archimedes' principle with ethanol as the immersing medium. The relative density of each sintered material was evaluated by the ratio between the measured density and the theoretical density of the powders calculated from the initial compositions using the rule of mixture.

2.2. Oxidation

The oxidation of the samples in air plasma conditions at high temperature was carried out using the MESOX facility (Moyen d'Essai

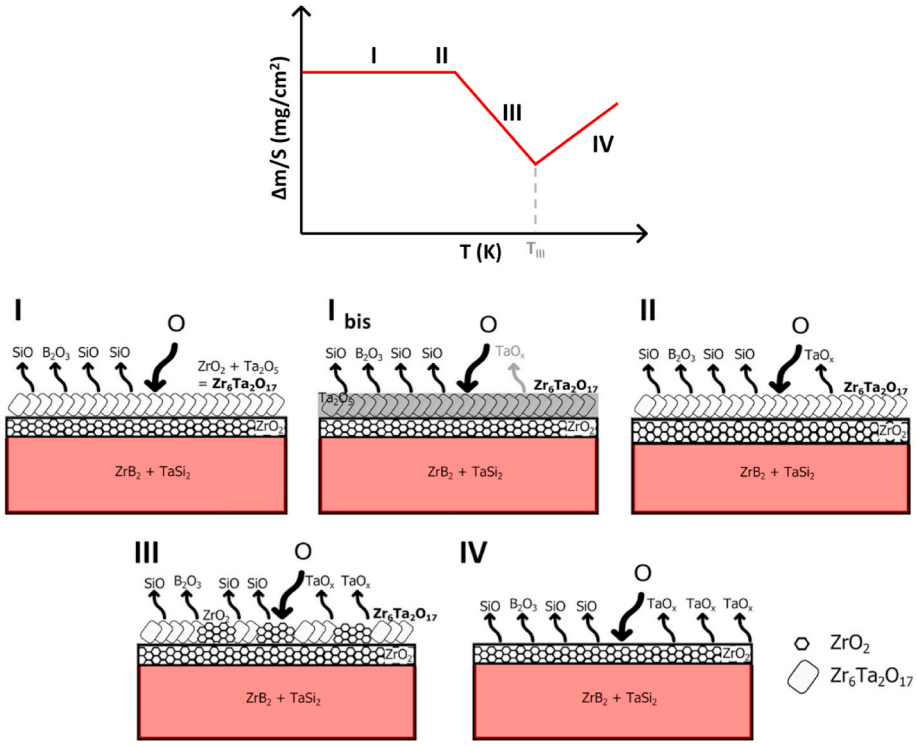

Fig. 13. Scheme of the proposed oxidation mechanisms.

Solaire d'Oxydation) placed at the focus of the 6 kW Odeillo solar furnace. The device is presented and detailed in a previous study [1]. The experimental parameters were chosen to partially reproduce the atmospheric re-entry conditions on Earth. The total pressure is fixed at 1000 Pa, representing a pressure encountered during the re-entry phase in between 80 and 60 km altitude where the dissociation of dioxygen to atomic oxygen occurs due to the high speed of the vehicle. A microwave air plasma is generated around the sample (300 W) containing about 70–80% of atomic oxygen [13]. The sample is placed in the quartz tube, the plasma is ignited then the shutter is opened and the temperature rise of the sample lasts only a few tens of seconds to reach a plateau at the targeted temperature, maintained during 300 s. The sample is then rapidly cooled down by closing the shutter and stopping the plasma. The study was conducted over a temperature range from 1950 K to 2600 K. The samples are weighed before and after oxidation using a precise balance (Ohaus Adventurer AX224, 0.1 mg accuracy).

2.3. Normal emissivity measurement

Emissivity measurement in air conditions at low pressure (1000 Pa) on pre-oxidized samples have been made in the original experimental set-up MEDIASE implemented at the focus of the 1 MW solar furnace and detailed in a previous study [14]. The direct method used at PROMES-CNRS laboratory is the one that corresponds directly to the definition of the emissivity: the directional spectral radiance (L'_λ) of the material is measured as well as its temperature to calculate the spectral radiance of the blackbody (L^0_λ) at the same temperature. The ratio of the radiances gives the spectral directional emissivity:

$\varepsilon'_\lambda = L'_\lambda / L^0_\lambda$ In this study, due to the size of the samples (25 mm diameter), only the normal spectral emissivity was measured and the normal total emissivity was calculated by integration of the spectral values.

2.4. Material characterization

Scanning Electron Microscopy (SEM) and Energy Dispersive Spectroscopy (EDS) analysis were done using a Hitachi S-4500 SEM-FEG microscope. X-ray diffraction (XRD) analysis was performed using a PANalytical XPert Pro diffractometer (Cu Kα radiation, $\lambda = 1.5418$ Å). X-ray diffraction measurements of θ-θ symmetrical scans were made over an angular range of 20–70° in 2θ. The step size and the time per step were fixed at 0.017° and 10 s, respectively. The X-ray diffractograms were recorded and studied using PANalytical softwares (Data collector and HighScorePlus). Raman measurements were performed using a micro-Raman spectrometer (LabRAM HR Evolution, HORIBA Scientific, France). Raman spectra were collected along the cross-section of the oxidized sample. A 633 nm laser was used for ZrB_2-based samples due to the luminescence phenomenon caused by zirconia formation and a 532 nm laser was used for HfB_2-based samples.

3. Experimental results and discussion

In this section, the material characterization of the sintered samples and the experimental results for oxidation are presented followed by a possible explanation of the oxidation mechanisms. Total normal emissivity measurements up to 2200 K are also given.

3.1. Characterization of the sintered samples

After SPS, the samples were characterized by SEM and XRD. The SEM pictures (Fig. 1) show no porosity on the surface of the polished samples, the pores visible on the H80T20 sample correspond to a grain pull-out during polishing. The maximal densities (100 %) were confirmed by Archimede's measures. No grain growth is observed certainly due to the sintering method and to the optimized sintering parameters with $TaSi_2$ as additional compound. The HfB_2 and ZrB_2 grains have relatively similar sizes. The diboride grains are surrounded by $TaSi_2$ suggesting that a liquid phase appeared during the process (Fig. 2). The formation of a liquid phase during the sintering process could explain the lower sintering temperatures than for the SiC-based composition by promoting a good densification. In this study, the relative density has been set carefully by adjusting the sintering parameters because it can affect the

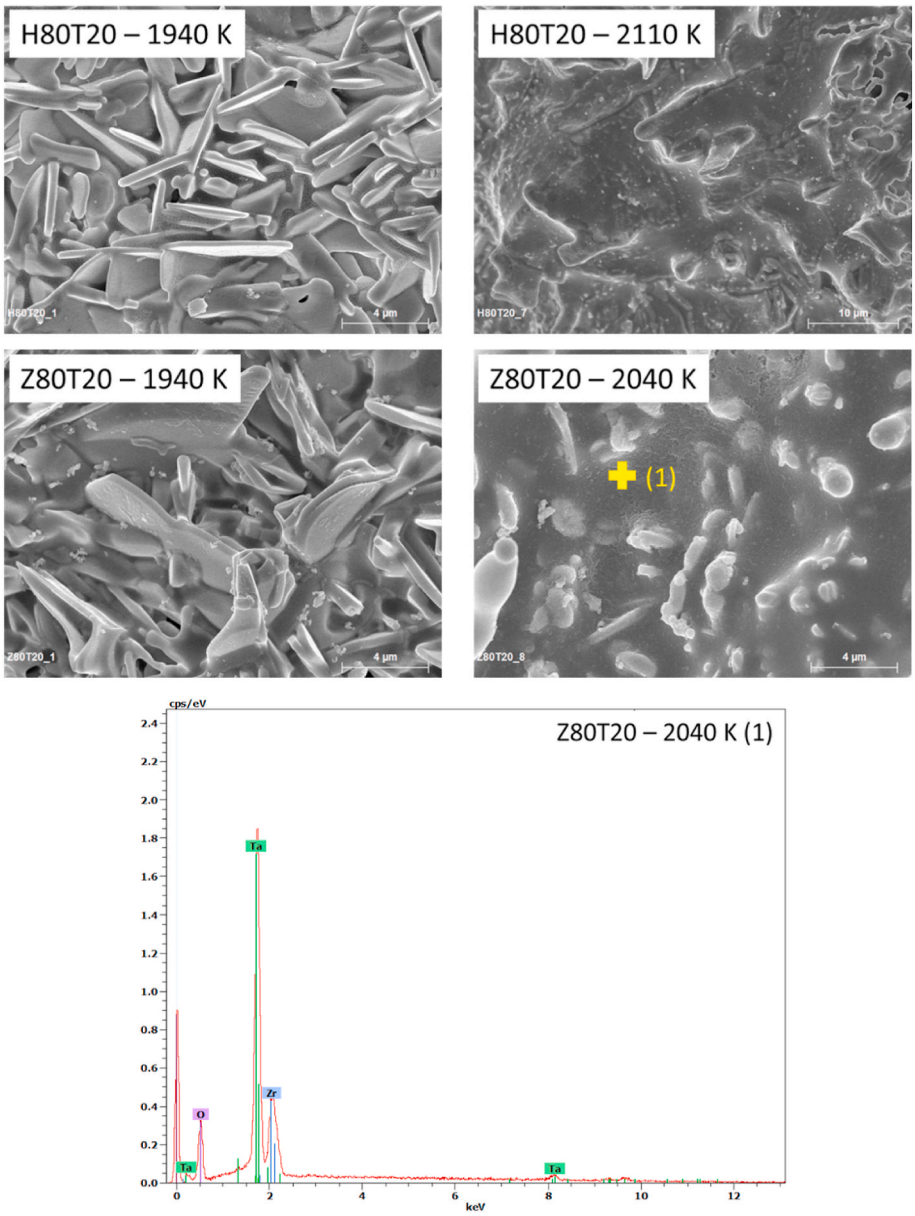

Fig. 14. SEM images from segment I and I_{bis} for the H80T20 and Z80T20 oxidized samples with EDS analysis (spot (1)).

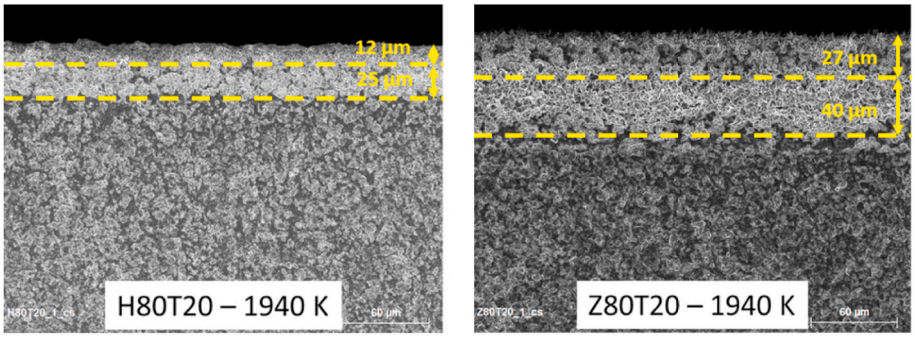

Fig. 15. SEM cross-sections of the H80T20 and Z80T20 samples oxidized at 1940 K.

oxidation resistance.

Fig. 3 presents the XRD patterns for the H80T20 and Z80T20 samples after sintering. The primary phases identified are the diborides, HfB_2 (ICDD 038-1398) or ZrB_2 (ICDD 034-0423), both hexagonal, and $TaSi_2$ (ICDD 072-6186) used as additional compound. However, a secondary phase, HfC (ICDD 039-1491), considered as negligible, has been detected for the hafnium-based composite due to the impurities present in the initial HfB_2 powder. For the Z80T20 sample, a $(Zr,Ta)B_2$ solid solution

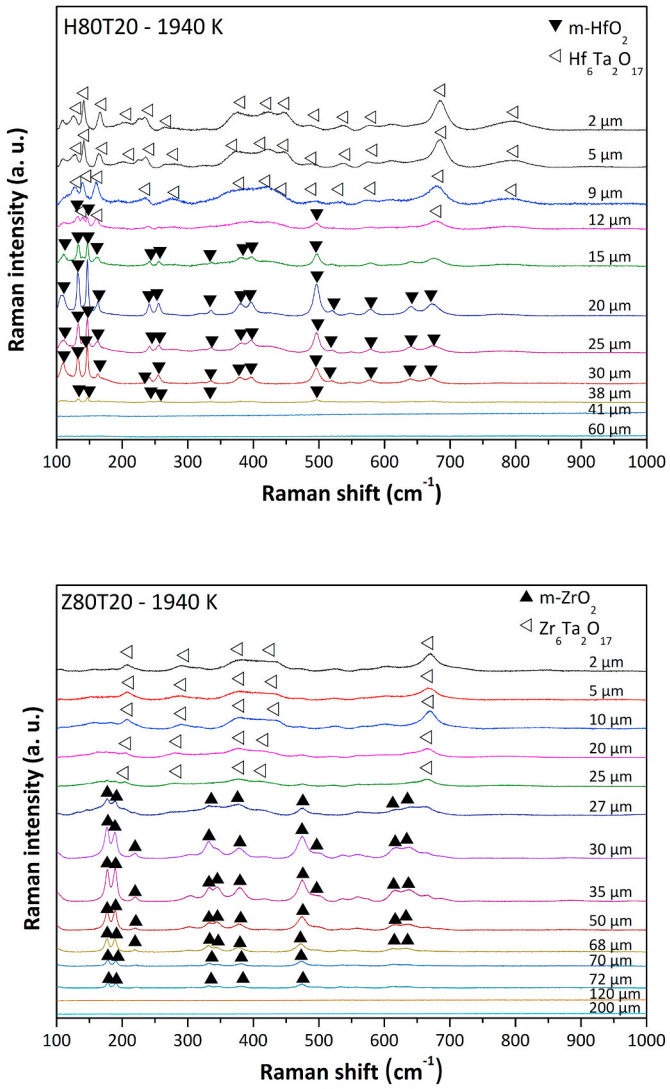

Fig. 16. Raman spectra obtained on the cross-sections of the H80T20 and Z80T20 samples oxidized at 1940 K corresponding to the SEM images in Fig. 15.

(ICDD 089-3919) has been detected with split peaks due to the introduction of tantalum in the crystal lattice. The formation of a solid solution may be the reason for the more efficient sintering and could explain the lower sintering temperatures compared to SiC. For the H80T20 composite, a slight broadening at the basis of the diboride peaks could be a sign that a small amount of tantalum has been inserted into the HfB_2 lattice. It can be noted that a) the atomic radii of Zr (1.55 Å), Hf (1.55 Å) and Ta (1.45 Å) are very close, b) the borides have the same crystal structure (hexagonal system, P6/mmm space group), and c) a solid solution is highly probable as presented in Fig. 4. The formation of a solid solution during the sintering process has been already observed by Talmy et al. and Silvestroni et al. on (Hf/ZrB_2)–$TaSi_2$ composites sintered by HP [15–17].

3.2. Mixed oxide synthesis

As no Raman data currently exists in the literature for the $Hf_6Ta_2O_{17}$ and $Zr_6Ta_2O_{17}$ mixed oxides, two methods have been used. First, acquisitions were made on the surface of some oxidized (Hf/Zr)B_2–$TaSi_2$ samples where the only formed phase is the mixed oxide. Secondly, mixed oxides were sintered in the MESOX facility using the following protocol. HfO_2 or ZrO_2 and Ta_2O_5 powders in the 86 mol.% HfO_2 and 14 mol.% Ta_2O_5 proportions have been ball-milled in a planetary miller for 5 min. Mixtures were introduced in a die (inner diameter 15 mm) and pre-compacted at 1 ton to form a pellet. Then, the sintering step has been made using the MESOX facility (without microwaves) at 1940 K during 5 min holding time at 8000 Pa total pressure for both the compositions. XRD patterns of these samples after sintering are presented in Fig. 5. For both the compositions, the major phase is $Zr_6Ta_2O_{17}$ or $Hf_6Ta_2O_{17}$ respectively. Secondary phases have been detected, Ta_2O_5 on the Zr-based oxide and HfO_2 on the Hf-based mixed oxide. The positions of the peaks determined for the $Hf_6Ta_2O_{17}$ mixed oxide are: 112, 130, 144, 165, 194, 240, 282, 331, 376, 395, 422, 498, 537, 573, 611, 686 and 795 cm^{-1} (Fig. 6 a)). The hafnia spectrum is still visible on the HfO_2-Ta_2O_5 sample sintered at 1940 K as in the XRD pattern (Fig. 5). The peak positions determined for the $Zr_6Ta_2O_{17}$ mixed oxide are: 107, 144, 179, 207, 291, 315, 378, 408, 436, 471, 527, 571, 601, 670, and 792 cm^{-1} (Fig. 6 b)). Similar Raman spectra, for the $Zr_6Ta_2O_{17}$ mixed oxide, to those obtained in this study have been reported in the literature but the positions of the peaks were not reported by the authors [19,20].

3.3. Oxidation at high temperature in air plasma

The oxidation study was performed on several samples for the two compositions, H80T20 and Z80T20, presented in Fig. 7. The reported temperatures for the Hf-based and Zr-based composites could be a little bit different due to the heating mode using concentrated solar energy. The mass variation by unit area was measured between the beginning and the end of the oxidation test and has been reported in Fig. 8 in the 1940–2610 K temperature range. In Fig. 8, the results obtained for the SiC counterparts detailed in a previous study, H80S20 and Z80S20, are also plotted in gray levels for comparison [1].

Fig. 9 and Fig. 10 show the XRD patterns of the H80T20 oxidized samples from 1940 K up to 2450 K and the Z80T20 oxidized samples from 1940 K up to 2610 K respectively. From 1940 K to 2180 K, for both the compositions, the only phase is the mixed oxide, $Hf_6Ta_2O_{17}$ (ICDD 044-0998) or $Zr_6Ta_2O_{17}$ (ICDD 042-0060) depending on the type of the initial diboride. From 2260 K to 2390 K for H80T20 and from 2360 K up to 2500 K for Z80T20, the monoclinic hafnia and zirconia phases are identified as major phases with respective mixed oxides as secondary phases. The proportion of the mixed oxides decreases with the increasing temperature. At the maximum temperatures reached, 2450 K for H80T20 and 2610 K for Z80T20, the only remaining phase is m-HfO_2 or m-ZrO_2 respectively. To summarize, the phases identified by XRD after oxidation as a function of temperature and initial composition are shown in Fig. 11. The identified phases for H80T20 and Z80T20 samples are essentially the same but the temperature ranges differ at some points. It appears that the $Zr_6Ta_2O_{17}$ mixed oxide is present in a wider temperature range than $Hf_6Ta_2O_{17}$. $Hf_6Ta_2O_{17}$ is no longer detected at 2450 K while its melting temperature of 2523 K has not been attained. About the melting temperature of the Zr-based mixed oxide, no information is available at this time in the literature, but it was detected up to 2500 K so it seems that its melting temperature could be higher than this value.

In order to identify the oxidation mechanisms, the interpretations were based on a phase diagram. A theoretical ZrO_2–Ta_2O_5 phase diagram proposed by Bhattacharya et al. exists but thermodynamic data are not available for the $Zr_6Ta_2O_{17}$ mixed oxide [21]. As Hf- and Zr- based oxides have similar behaviors (HfO_2 and ZrO_2), the same is assumed in this study for the respective mixed oxides with Ta. The interpretations will be based on the experimental HfO_2-Ta_2O_5 diagram recently established by Mc Cormack et al. (Fig. 12) that reports the domains of existence of the mixed oxide [4].

Fig. 13 details the three segments of the mass variation versus temperature and the four associated oxidation mechanisms. These mechanisms are explained in the following sections with corresponding SEM images and Raman spectroscopy analysis. The different oxidation mechanisms have been separated into four segments according to the

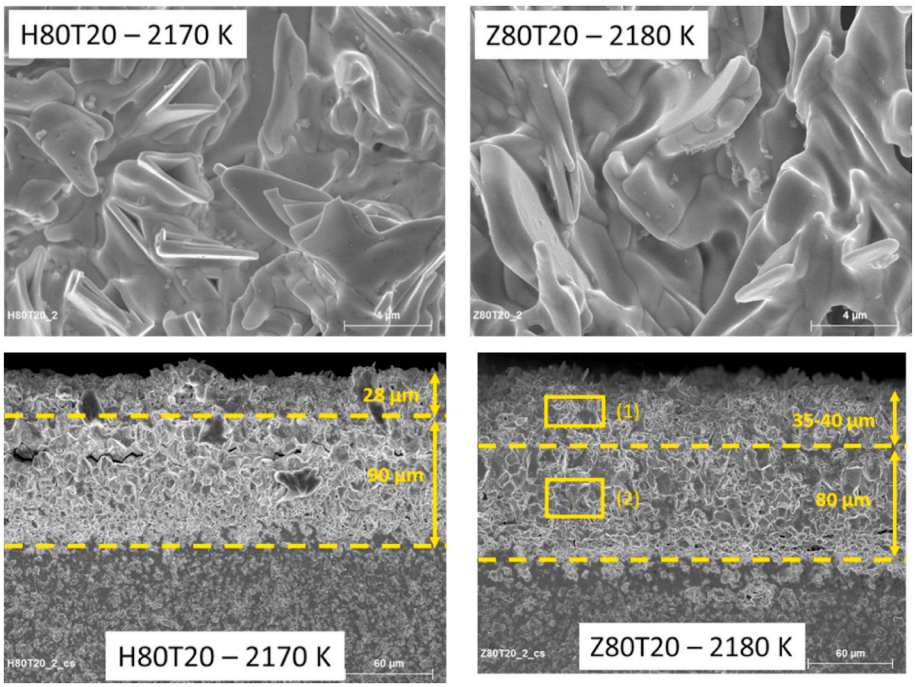

Fig. 17. SEM images from segment II for the H80T20 and Z80T20 oxidized samples.

mass variation and the associated chemical reactions.

The four segments are defined as follows:

- Segments I and I_{bis}: from 1940 K to 2110 K, a slight mass gain with typical crystals and a liquid phase are observed on the surface with the increase of temperature (Segment I_{bis}). The eutectic temperature given by Mc Cormack et al. for the formation of a liquid is 2004 ± 34 K. The highest temperature at which a liquid phase was observed in this study is around 2110 K on the H80T20 sample. The segment I_{bis} is therefore defined from 2004 K (temperature of the liquid phase formation) to 2110 K (highest temperature observed for the liquid phase),
- Segment II: from 2110 K to 2170 K, this segment is characterized by a slight mass gain and the disappearance of the liquid phase,
- Segment III: from 2170 K to T_{III}, this segment is defined by a first important mass loss with the coexistence of the mixed oxide and zirconia or hafnia on the surface. The two temperatures, 2310 K for H80T20 and 2500 K for Z80T20, are referred to T_{III} hereafter since the same reactions are associated with them but they occur at different temperatures according to the initial composition,
- Segment IV: from T_{III} to T_{max}, this segment corresponds to a mass recovery and the total disappearance of the mixed oxide from the surface with only hafnia or zirconia remaining.

3.3.1. *Segment I and I_{bis}: 1940 K to 2110 K*

In the segment I, from 1940 K to 2110 K, a slight mass gain is observed for both the compositions. The mass gain is attributed to the formation of a mixed oxide on the surface. The typical shape (platelets) of this phase is visible in Fig. 14 for both the compositions.

Fig. 14 shows the SEM images of the surfaces of the H80T20 and Z80T20 samples oxidized at 1940 K and 2110 K, 1940 K and 2040 K respectively. The microstructures are very similar for both the compositions at the same temperature levels. At 1940 K, platelet-like crystals characteristic of the $Hf_6Ta_2O_{17}$ or $Zr_6Ta_2O_{17}$ mixed oxides are visible [17]. These observations are confirmed by XRD analysis that shows only the mixed oxide peaks at these temperatures (Fig. 9). It appears that HfO_2 or ZrO_2 formed by oxidation react with Ta_2O_5 to form the mixed oxides $Hf_6Ta_2O_{17}$ or $Zr_6Ta_2O_{17}$ according to reactions (1) to (6).

$$HfB_2(s) + 5\ O(g) \rightarrow HfO_2(s) + B_2O_3(l,g) \quad (1)$$

$$ZrB_2(s) + 5\ O(g) \rightarrow ZrO_2(s) + B_2O_3(l,g) \quad (2)$$

$$2\ TaSi_2(s) + 7\ O(g) \rightarrow Ta_2O_5(s,l) + SiO_2(l,s) \quad (3)$$

or

$$2\ TaSi_{\ 2}(s) + 6\ O(g) \rightarrow Ta_2O_5(s,l) + SiO(g) \quad (4)$$

$$6\ HfO_2 + Ta_2O_5 \rightarrow Hf_6Ta_2O_{17} \quad (5)$$

$$6\ ZrO_2 + Ta_2O_5 \rightarrow Zr_6Ta_2O_{17} \quad (6)$$

With the temperature increase, at 2040 K and 2110 K for Z80T20 and H80T20 samples respectively, a liquid phase covers the surface (Fig. 14). From 1940 K to 2004 K, the reactions occur in the $Ta_2O_5 + Hf_6Ta_2O_{17}$ zone (Segment I, Fig. 12) of the phase diagram and with the increase of the temperature, a liquid phase appears (Segment I_{bis}). To identify the liquid phase formed on the surface at 2040 K, EDS analyses were performed and presented in Fig. 14 (spot 1). It appears that this phase is mainly composed of Ta and O with a small quantity of Zr. We supposed that this area is composed of molten Ta_2O_5 with $Zr_6Ta_2O_{17}$ mixed oxide crystals underneath. The same assumption can be made for the hafnium-based sample oxidized at 2110 K. The thicknesses of the oxidized layers are 40 µm and 70 µm for H80T20 and Z80T20 respectively, both oxidized at 1940 K (Fig. 15). Raman spectroscopy analyses were conducted along the cross-sections to identify the phases. Fig. 16 shows the Raman spectra obtained on the cross-sections of H80T20 and Z80T20 samples oxidized at 1940 K corresponding to the SEM images presented in Fig. 15. It appears that from 12 µm or 27 µm respectively, $Hf_6Ta_2O_{17}$ or $Zr_6Ta_2O_{17}$ mixed oxides have been identified. Deeper in the cross-section, monoclinic hafnia or zirconia is visible. The thickness of the oxide layer of Z80T20 sample is thicker than for H80T20 sample although the slight mass gain on segment I is the same.

3.3.2. *Segment II: 2110 K to 2180 K*

At the end of the I_{bis} segment (2110 K), a partial vaporization/sublimation of $Ta_2O_5(s,l)$ occurs. The phenomenon is clearly visible on the

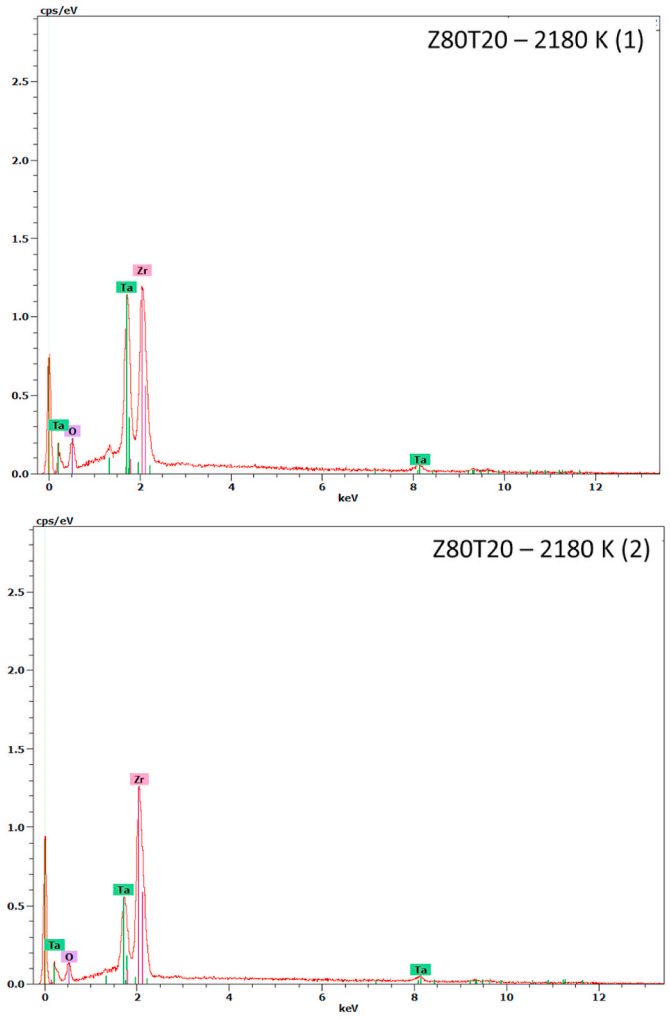

Fig. 18. EDS analysis on the areas marked in Fig. 17 on the Z80T20 oxidized sample.

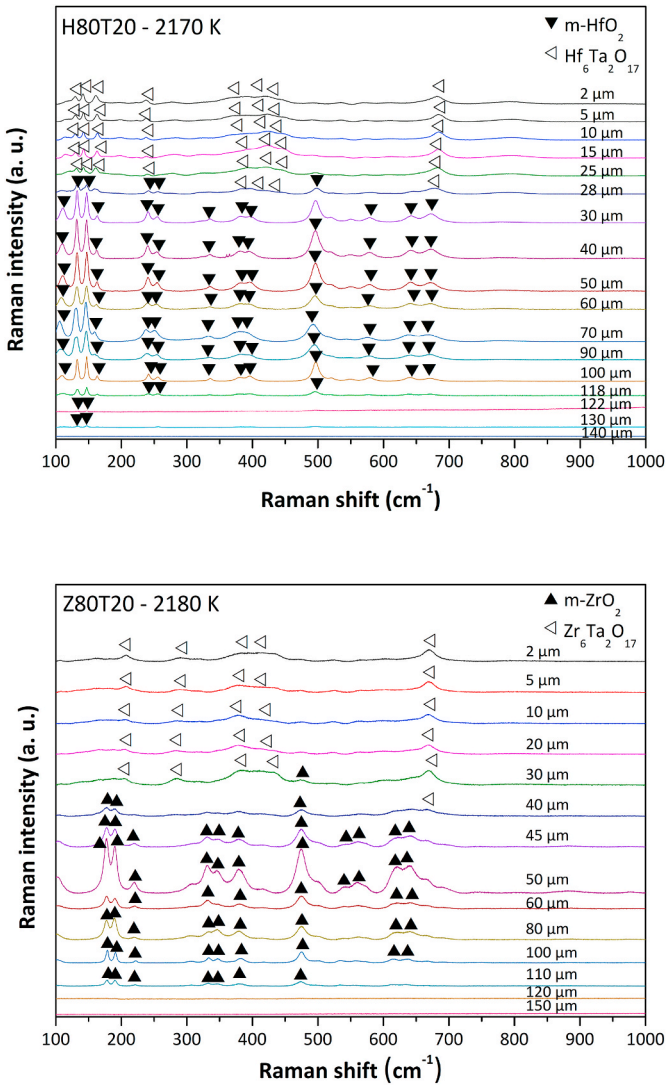

Fig. 19. Raman spectra obtained on the cross-sections of the H80T20 and Z80T20 samples oxidized at 2180 K corresponding to the SEM images in Fig. 17.

H80T20 sample oxidized at 2110 K with some porosities in the liquid phase formed on the surface (Fig. 14). As soon as a liquid phase appears on the surface, volatilization begins due to the low total pressure inside the reactor during the oxidation experiments. The two main products of Ta_2O_5 vaporization are TaO(g) and TaO_2(g), grouped under the TaO_x(g) generic term in Fig. 13. The proportion of Ta_2O_5 at the surface tends to decrease and the reaction shifts to a larger proportion of HfO_2 (or ZrO_2) in the phase diagram (Fig. 12, segment II). At 2170 K, the surfaces show crystals of typical shape attesting the presence of the mixed oxide (Fig. 17). However, these crystals are no longer as well defined as for the samples oxidized at 1940 K, the grains being more stucked together. Moreover, the liquid phase present on the I_{bis} segment (at 2040 K for Z80T20 and 2110 K for H80T20) is no longer visible. These observations are confirmed by the XRD analysis with only mixed oxides detected. It is clear that on the surface there is less Ta_2O_5 compared to the molar fraction of 0.26 initially present, because at this temperature, the liquid phase would be visible. Segment II corresponds to the area where the mixed oxide is the only one formed as observed experimentally by XRD analysis and SEM imaging.

Despite the partial vaporization/sublimation of Ta_2O_5 into TaO_x(g), a mass gain is still observed on this segment due to the formation of denser oxides compared to the initial borides. Moreover, on this segment, the thickness of the oxide layer is greater, around 120 µm, for both the compositions than in segment I (Fig. 15). Raman spectroscopy was performed to determine the phases present along the cross-sections.

It appears that up to 30 µm for H80T20 and 35–40 µm for Z80T20, the mixed oxide has been identified. Then, down to 120 µm, hafnia or zirconia is respectively present (Fig. 19). These observations are confirmed by EDS analysis presented in Fig. 18 with Ta observed at the extreme surface (1) and in minor quantity deeper in the cross-section (2). EDS analysis on H80T20 samples are not presented because the peaks of Hf and Ta are overlapped and prevent any conclusion. It seems that Ta is only present at the extreme surface of the oxidized layers, either in segment I or II. It is possible that Ta migrates from the bulk to the surface during the oxidation process.

3.3.3. *Segment III: 2180 K to T_{III}*

According to the XRD analysis, the proportion of the mixed oxide decreases with the increase of the temperature on this segment and the proportion of hafnia or zirconia increases. It appears that the proportion of Ta_2O_5 decreases involving a decreasing of the proportion of the mixed oxides formed. The two temperatures, different according to the composition, 2310 K for H80T20 and 2500 K for Z80T20, are referred to T_{III} hereafter since the same reactions are associated. The zone in the phase diagram associated to this segment III is the one with the presence of t-HfO_2 (or t-ZrO_2) and $(Hf/Zr)_6Ta_2O_{17}$ (Segment III, Fig. 12). The t-HfO_2 and t-ZrO_2 oxides were found in their monoclinic forms because

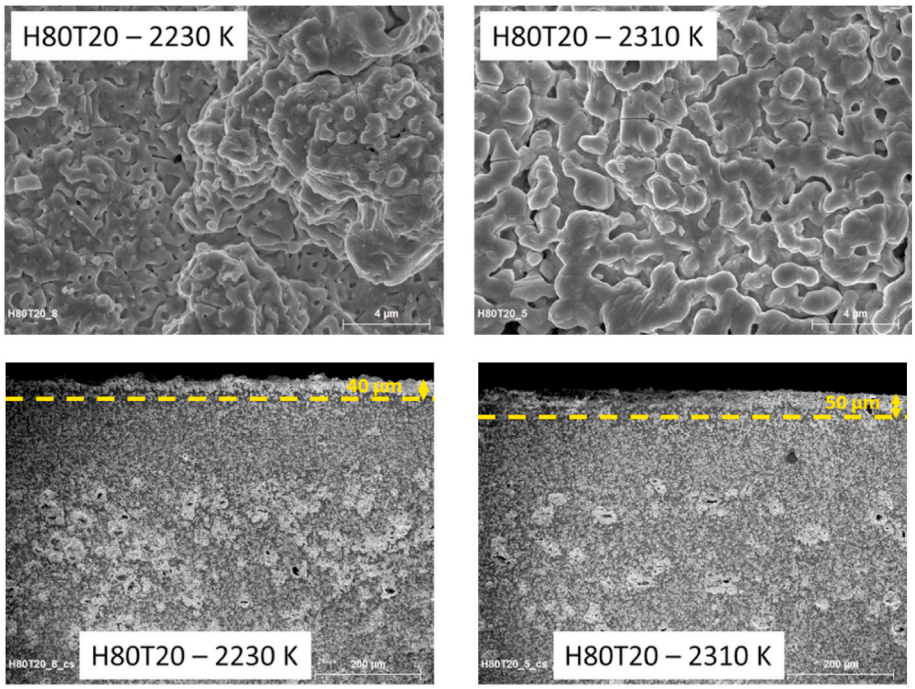

Fig. 20. SEM images of the H80T20 oxidized samples in the segment III (surfaces and corresponding cross-sections).

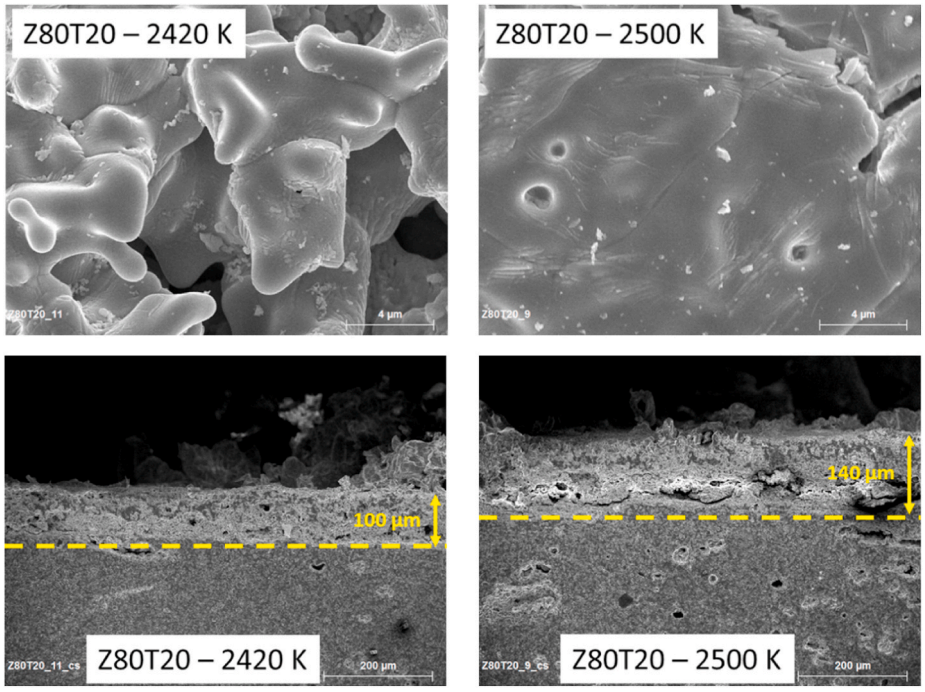

Fig. 21. SEM images of the Z80T20 oxidized samples in the segment III (surfaces and corresponding cross-sections).

the phase transformation is reversible during the cooling.

3.3.3.1. H80T20 samples. From 2230 K to 2310 K, the crystals have a similar shape and their size increases with temperature (Fig. 20). The oxidized layers are relatively thin on this segment, between 40 and 50 µm, but the mass losses are important certainly due to vaporization phenomena. Moreover, on the cross-section images of the samples in the segment III, porosities appear in the depth, well below the oxidized layer. Three zones are visible: a layer composed of oxide (hafnia and mixed oxide), a layer that seems denser and a very extensive layer with porosities. One possible explanation is that some $TaSi_2$ has migrated to the surface and vaporized leaving porosities inside the material.

3.3.3.2. Z80T20 samples. From 2170 K, a mass loss is observed attesting a vaporization phenomenon. At 2420 K, crystals are visible and at 2500 K the surface appears to be composed of bigger crystals (Fig. 21). It seems that the oxidation mechanisms involved for the two compositions, Z80T20 and H80T20, are very similar but slightly shifted in temperature.

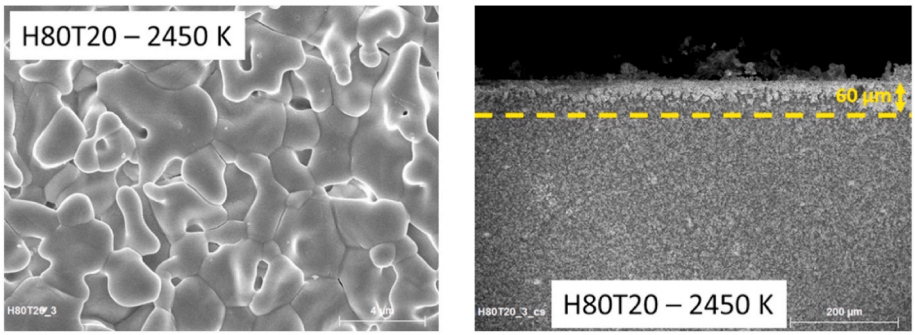

Fig. 22. SEM images of the H80T20 sample oxidized at 2450 K (surface and corresponding cross-section).

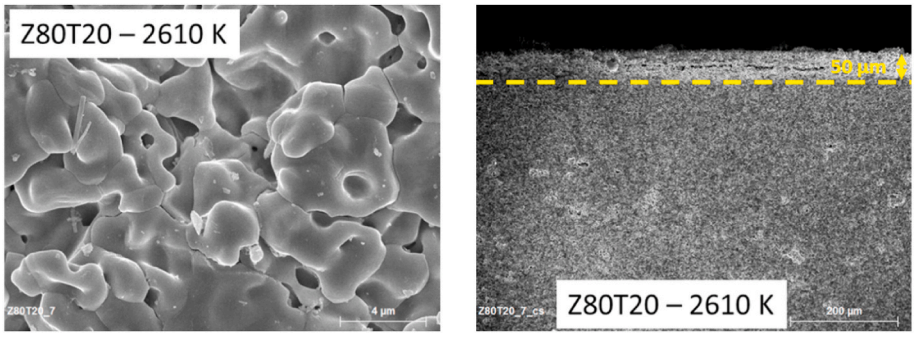

Fig. 23. SEM images of the Z80T20 sample oxidized at 2610 K (surface and corresponding cross-section).

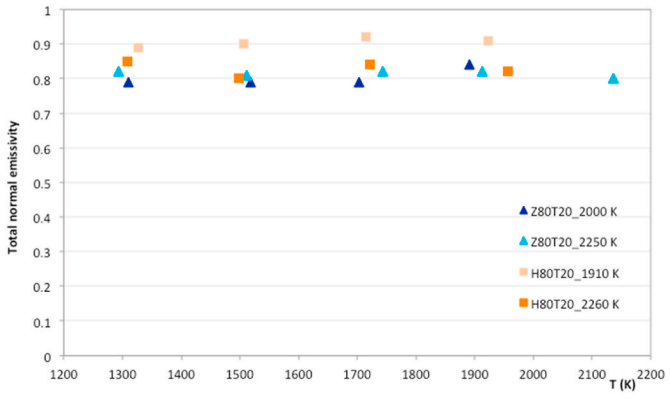

Fig. 24. Total normal emissivity versus temperature at 1000 Pa air. The temperature indicated in the caption referred to the temperature of the pre-oxidation in the MESOX set-up.

3.3.4. *Segment IV: T_{III} to T_{max}*

The H80T20 sample was oxidized at a lower temperature than the Z80T20 one. Solar experiments did not allow reaching temperatures higher than 2450 K for the H80T20 composition. The segment IV is characterized by a mass recovery and the complete disappearance of the mixed oxide. These phenomena do not appear at the same temperature according to the initial composition: at 2450 K for H80T20 and 2610 K for Z80T20. The complete disappearance of the mixed oxide occurs leaving only hafnia or zirconia grains on the surface (Fig. 22 and Fig. 23) where the characteristic shape of these crystals is visible. A possible explanation would be that, at these temperature levels, Ta_2O_5 is directly vaporized and only hafnia or zirconia would form on the surface in a dense layer that protects the material more efficiently from oxidation. The thicknesses of the oxide layer as well as the mass losses are lower on the segment IV than on the segment III (Figs. 22 and 23).

At these temperature levels, the thickness of the oxidized layer is very low: about 50–60 µm for both the compositions. Volatilization phenomena still occurred because the mixed oxide is not formed and a mass loss is observed for both the compositions. However, it is much lower than for its SiC counterparts: -3.37% for Z80S20 and -1.06% for Z80T20, both of them being oxidized at 2600 K. A very small mass loss was observed for H80T20 at 2450 K. However, the solar experiments did not allow to go higher in temperature for HfB_2-based composites, it is thus difficult to conclude on the behavior at around 2600 K. But, the H80S20 oxidized sample presents a very important mass loss (−1.56%) at 2400 K and the H80T20 oxidized sample presents a slight mass loss at 2450 K (−0.09%). It appears that $TaSi_2$ does not avoid a significant mass loss at very high temperature (Segment III) but it is considerably reduced compared to those observed on (Zr/Hf)B_2–SiC composites. Plus, the replacement of SiC by $TaSi_2$ is beneficial up to 2170 K that is 200 K beyond SiC-based composites that have presented a significant mass loss from 2000 K.

3.4. *Normal total emissivity*

Before the emissivity measurement, the samples were pre-oxidized in the MESOX set-up in air plasma to obtain a similar surface in terms of microstructure and chemical composition than those obtained in the oxidation study. Data obtained for the total normal emissivity versus temperature at 1000 Pa total air pressure for the two different compositions, Z80T20 and H80T20, are presented in Fig. 24. The total normal emissivity is quite constant in the temperature range for the two compositions considering the uncertainty (5%). The emissivity is around 0.85–0.90 for HfB_2-based composite, and 0.80 for ZrB_2-based material.

The only other study that report measurements of the total hemispherical emissivity at high temperature is the one conducted by Justin and Jankoviak up to 1073 K on pre-oxidized (Zr/Hf)B_2-20 vol% SiC-20 vol% $TaSi_2$ samples at 1273 K [2]. The emissivity values obtained were greater than 0.80, just like in our study, but at lower temperatures.

4. Conclusion

Fully-dense (Hf/Zr)B_2-20 vol% $TaSi_2$ samples were sintered by SPS. The introduction of $TaSi_2$ into (Hf/Zr)B_2-based composites has improved their oxidation resistance compared to the addition of SiC. The protection against oxidation generated by the replacement of SiC by $TaSi_2$ is clearly visible and beneficial up to 2170 K that is 200 K beyond SiC. A slight mass gain accompanied by a relatively thin oxidized layer compared to the SiC compositions has been observed up to this temperature. A four-step oxidation mechanism has been proposed:

- Segments I and I_{bis}: from 1940 K to 2110 K, a slight mass gain was measured, with the presence of a mixed oxide - $Zr_6Ta_2O_{17}$ or $Hf_6Ta_2O_{17}$ - on the surface and a liquid phase composed of molten Ta_2O_5 with mixed oxide crystals underneath, with the increase of temperature (Segment I_{bis}),
- Segment II: from 2110 K to 2170 K, this segment is characterized by a slight mass gain and the disappearance of the liquid phase,
- Segment III: from 2170 K to T_{III}, a first mass loss was observed with the coexistence of the mixed oxide and zirconia or hafnia on the surface due to the vaporization of Ta_2O_5,
- Segment IV: from T_{III} to T_{max}, a mass recovery in observed and only a dense hafnia or zirconia layer remains on the surface. A possible explanation could be that the rapid formation of a compact hafnia or zirconia layer better protects the material against oxidation than with SiC as adding component.

As no data exists in the literature at such high temperatures and as it is an important parameter to know for the atmospheric re-entry on Earth of a space vehicle, the normal spectral emissivity of pre-oxidized samples was measured and values of 0.85–0.90 for the HfB_2-based composite and 0.80 the for ZrB_2-based material were obtained.

Even if the replacement of SiC by $TaSi_2$ has improved the oxidation resistance up to 2200 K, it is not the ideal candidate for atmospheric re-entry applications at high velocity, due to the important mass loss at this temperature caused by the vaporization of Ta_2O_5. Moreover, the presence of silicon leads to vaporization phenomenon from 2000 K and potentially to porosities. In order to avoid the presence of silicon, the replacement of SiC or $TaSi_2$ by AlN is under study.

Declaration of competing interest

The authors declare that they have no known competing financial interests or personal relationships that could have appeared to influence the work reported in this paper.

Acknowledgments

The authors want to thank J.L. Sans from PROMES-CNRS lab for the emissivity measurements and M. Vandenhende from IRCER lab for the technical support during the sintering process. This work was partially funded by the Région Occitanie under the contract number 2018001076 ALDOCT-000472, CNRS n° 173239 and FEDER-FSE under the contract number 2018-001076-01, CNRS n°179222 through the PhD funding of C. Pellegrini.

References

[1] C. Pellegrini, M. Balat-Pichelin, O. Rapaud, E. Bêche, Oxidation resistance of Zr- and Hf-diboride composites containing SiC in air plasma up to 2600 K for aerospace applications, Ceram. Int. 48 (2022) 2177–2190, https://doi.org/10.1016/j.ceramint.2021.09.310.
[2] J.F. Justin, A. Jankowiak, Ultra high temperature ceramics: densification, properties and thermal stability, J. Aerospace Lab. (2011) 1–11.
[3] E. Opila, S. Levine, J. Lorincz, Oxidation of ZrB_2 - and HfB_2 -based ultra-high temperature ceramics: effect of Ta additions, J. Mater. Sci. 39 (2004) 5969–5977, https://doi.org/10.1023/B:JMSC.0000041693.32531.d1.
[4] S.J. McCormack, K. Tseng, R.J.K. Weber, D. Kapush, S.V. Ushakov, A. Navrotsky, W.M. Kriven, In-situ determination of the HfO_2 –Ta_2O_5 temperature phase diagram up to 3000°C, J. Am. Ceram. Soc. 102 (2019) 4848–4861, https://doi.org/10.1111/jace.16271.
[5] M. Gasch, S. Johnson, Physical characterization and arcjet oxidation of hafnium-based ultra high temperature ceramics fabricated by hot pressing and field-assisted sintering, J. Eur. Ceram. Soc. 30 (2010) 2337–2344, https://doi.org/10.1016/j.jeurceramsoc.2010.04.019.
[6] E.P. Simonenko, N.P. Simonenko, A.N. Gordeev, A.F. Kolesnikov, A.V. Chaplygin, A.S. Lysenkov, I.A. Nagornov, V.G. Sevastyanov, N.T. Kuznetsov, Oxidation of HfB_2-SiC-Ta_4HfC_5 ceramic material by a supersonic flow of dissociated air, J. Eur. Ceram. Soc. 41 (2021) 1088–1098, https://doi.org/10.1016/j.jeurceramsoc.2020.10.001.
[7] L. Silvestroni, G. Meriggi, D. Sciti, Oxidation behavior of ZrB_2 composites doped with various transition metal silicides, Corrosion Sci. 83 (2014) 281–291, https://doi.org/10.1016/j.corsci.2014.02.026.
[8] I.G. Talmy, J.A. Zaykoski, M.M. Opeka, A.H. Smith, Properties of ceramics in the system ZrB_2–Ta_5Si_3, J. Mater. Res. 21 (2006) 2593–2599, https://doi.org/10.1557/jmr.2006.0321.
[9] I.G. Talmy, J.A. Zaykoski, M.M. Opeka, High-temperature chemistry and oxidation of ZrB_2 ceramics containing SiC, Si_3N_4, Ta_5Si_3, and $TaSi_2$, J. Am. Ceram. Soc. 91 (2008) 2250–2257, https://doi.org/10.1111/j.1551-2916.2008.02420.x.
[10] L. Silvestroni, H.-J. Kleebe, Critical oxidation behavior of Ta-containing ZrB_2 composites in the 1500–1650 °C temperature range, J. Eur. Ceram. Soc. 37 (2017) 1899, https://doi.org/10.1016/j.jeurceramsoc.2017.01.020. –1908.
[11] P. Hu, X.-H. Zhang, J.-C. Han, X.-G. Luo, S.-Y. Du, Effect of various additives on the oxidation behavior of ZrB_2-based ultra-high-temperature ceramics at 1800°C, J. Am. Ceram. Soc. 93 (2010) 345–349, https://doi.org/10.1111/j.1551-2916.2009.03420.x.
[12] D. Sciti, V. Medri, L. Silvestroni, Oxidation behaviour of HfB_2–15 vol.% $TaSi_2$ at low, intermediate and high temperatures, Scripta Mater. 63 (2010) 601–604, https://doi.org/10.1016/j.scriptamat.2010.05.050.
[13] M. Balat-Pichelin, A. Vesel, Neutral oxygen atom density in the MESOX air plasma solar furnace facility, Chem. Phys. 327 (2006) 112–118, https://doi.org/10.1016/j.chemphys.2006.03.034.
[14] M. Balat-Pichelin, J.-L. Sans, E. Bêche, L. Charpentier, A. Ferrière, S. Chomette, Emissivity at high temperature of Ni-based superalloys for the design of solar receivers for future tower power plants, Sol. Energy Mater. Sol. Cells 227 (2021), 111066, https://doi.org/10.1016/j.solmat.2021.111066.
[15] I.G. Talmy, J.A. Zaykoski, M.M. Opeka, High-temperature chemistry and oxidation of ZrB_2 ceramics containing SiC, Si_3N_4, Ta_5Si_3, and $TaSi_2$, J. Am. Ceram. Soc. 91 (2008) 2250–2257, https://doi.org/10.1111/j.1551-2916.2008.02420.x.
[16] L. Silvestroni, D. Sciti, Densification of ZrB_2-$TaSi_2$ and HfB_2-$TaSi_2$ ultra-high-temperature ceramic composites, J. Am. Ceram. Soc. 94 (2011) 1920–1930, https://doi.org/10.1111/j.1551-2916.2010.04317.x.
[17] L. Silvestroni, H.-J. Kleebe, Critical oxidation behavior of Ta-containing ZrB_2 composites in the 1500-1650°C temperature range, J. Eur. Ceram. Soc. 37 (2017) 1899, https://doi.org/10.1016/j.jeurceramsoc.2017.01.020. –1908.
[18] F. Failamani, K. Göschl, G. Reisinger, C.A. Nunes, G.C. Coelho, A.J.S. Machado, L. E. Correa, J.C.P. dos Santos, G. Giester, P. Rogl, High temperature FeB-type phases in the systems Ta-{Ti,Zr,Hf}-B, J. Phase Equilibria Diffus. 36 (2015) 620–631, https://doi.org/10.1007/s11669-015-0418-y.
[19] J. Yuan, W. Song, H. Zhang, X. Zhou, S. Dong, J. Jiang, L. Deng, X. Cao, $TaZr_{2.75}O_8$ ceramics as a potential thermal barrier coating material for high-temperature applications, Mater. Lett. 247 (2019) 82–85, https://doi.org/10.1016/j.matlet.2019.03.102.
[20] Q. Liu, X. Hu, W. Zhu, J. Guo, Z. Tan, Effects of Ta_2O_5 content on mechanical properties and high-temperature performance of $Zr_6Ta_2O_{17}$ thermal barrier coatings, J. Am. Ceram. Soc. 104 (12) (2021) 6533–6544, https://doi.org/10.1111/jace.17990, jace, 17990.
[21] A.K. Bhattacharya, V. Shklover, W. Steurer, G. Witz, H. Bossmann, O. Fabrichnaya, Ta_2O_5–Y_2O_3–ZrO_2 system: experimental study and preliminary thermodynamic description, J. Eur. Ceram. Soc. 31 (2011) 249–257, https://doi.org/10.1016/j.jeurceramsoc.2010.09.009.